

# Pressure-induced deformation of the $C_{60}$ fullerene in $Rb_6C_{60}$ and $Cs_6C_{60}$

R. Poloni,<sup>1,2</sup> M. V. Fernandez-Serra,<sup>3</sup> S. Le Floch,<sup>2</sup> S. De Panfilis,<sup>1,4</sup> P. Toulemonde,<sup>2,5</sup> D. Machon,<sup>2</sup> W. Crichton,<sup>1</sup> S. Pascarelli,<sup>1</sup> and A. San-Miguel<sup>2</sup>

<sup>1</sup>European Synchrotron Radiation Facility, Boîte Postale 220, F-38043 Grenoble, France

<sup>2</sup>Université de Lyon, F-69000, France

and Université Lyon 1, Laboratoire PMCN, CNRS, UMR 5586, 69622 Villeurbanne, Cedex, France

<sup>3</sup>CECAM, ENS-Lyon, 46 Allée d'Italie, 69007 Lyon, France

<sup>4</sup>CRS-SOFT INFM-CNR, Università La Sapienza, Piazzale Aldo Moro 5, I-00185 Roma, Italy

<sup>5</sup>Institut Néel, Département MCMF, CNRS, Université Joseph Fourier, Boîte Postale 166, F-38042, Grenoble, France

(Received 20 July 2007; revised manuscript received 10 October 2007; published 22 January 2008)

We report a detailed experimental and theoretical study of the  $Rb_6C_{60}$  and  $Cs_6C_{60}$  systems under pressure. X-ray diffraction and x-ray absorption experiments have been coupled with *ab initio* calculations in order to understand the mechanisms taking place during the compression of these intercalated systems. The whole data set is consistent with a pressure-induced modification of the shape of the  $C_{60}$  molecule. This deformation constitutes an enhancement of the calculated distortion of the molecule in these intercalated compounds at ambient conditions, being equivalent to pulling the molecule through the three orthogonal axes pointing toward the bcc faces containing the alkali metals. Both experiments and calculations show that the pressure-induced deformation of the fullerene molecule is more important for Rb than it is for Cs intercalation.

DOI: 10.1103/PhysRevB.77.035429

PACS number(s): 61.48.-c, 61.05.cj, 61.05.cp, 61.50.Ah

## I. INTRODUCTION

The  $C_{60}$  fullerene and its compounds have attracted much attention due to some of their extraordinary properties, related to the high symmetry and simplicity of the molecule. Among the studied properties, the relative high superconducting critical temperature of alkali metal intercalated fullerenes has been one of the more remarkable. Additionally, the compressibility of a single buckminsterfullerene molecule is calculated to have values between 700 and 900 GPa,<sup>1,2</sup> exceeding significantly that of diamond. Subsequently, most studies of the high-pressure behavior of fullerene-based crystals have considered the molecule as not deformable up to the formation of intermolecular bondings. In fact, under high-pressure and high-temperature conditions, crystals of pristine  $C_{60}$ 's follow a series of phase transformations including the formation of one-dimensional, two-dimensional, or three-dimensional (3D) polymers which have been extensively studied.<sup>3-9</sup> Polymerization can lead to the deformation of the molecule;<sup>8,10</sup> nevertheless, a possible deformation of the noncovalently bonded  $C_{60}$  molecules under compression has not been detected yet. On the other side, the ionic interaction due to alkali intercalation has been predicted to give rise to a distortion of the  $C_{60}$ ,<sup>11</sup> compared to the isolated molecule. No experimental evidence of such deformation has been provided up to now. The application of pressure constitutes a possible means to enhance such distortion and its exploration constitutes the objective of the present work.

Intercalation with alkali metals can avoid or favor the formation of  $C_{60}$  intermolecular bonds depending on the nature and contents of intercalated atoms. Low content or low size of alkali atoms favor the formation of  $C_{60}$  polymers<sup>12-14</sup> which spontaneously form at ambient pressure. On the other hand, recent studies<sup>15</sup> have shown that for high Rb content, i.e., in  $Rb_6C_{60}$ , there is no phase transformation up to 22 GPa

and this makes of such system a very favorable case for the study of the evolution of the  $C_{60}$  molecule up to high pressures. Moreover, the intercalation with Cs, which is characterized by a bigger ionic radius, could stabilize the  $C_{60}$  molecule even more with respect to polymerization and act differently on the evolution of  $C_{60}$ 's geometry under pressure with respect to the Rb case. Consequently,  $Rb_6C_{60}$  and  $Cs_6C_{60}$  constitute good candidate systems for the study of the pressure evolution of the geometry of the  $C_{60}$  molecule. We have combined data from x-ray diffraction (XRD) and x-ray absorption (XAS) experiments with *ab initio* calculations to study the pressure evolution of the 60 carbon atom molecule in  $Rb_6C_{60}$  and  $Cs_6C_{60}$  as well as to probe the effect of the intercalated atom size on such evolution.

## II. EXPERIMENTAL DETAILS

The samples consisting of  $Cs_6C_{60}$  and  $Rb_6C_{60}$  powder compounds were prepared by mixing stoichiometric amounts of  $C_{60}$  (99.95% purity) with Cs and Rb (99.98% purity) metals in inert atmosphere, respectively. The final reaction was obtained by annealing the mixed powder closed in a sealed quartz tube at 500 K for a month. The quality of the sample was verified by XRD.

High-pressure experiments were performed at the European Synchrotron Radiation Facility (Grenoble, France) using a "Paris-Edinburgh" pressure device<sup>16</sup> with 5 mm sintered diamond anvils as described elsewhere.<sup>17</sup>

Angular dispersive XRD experiments were performed at the high-pressure insertion device ID27 beamline<sup>18</sup> by angle-resolved measurements. The monochromatic beam with wavelength  $\lambda=0.3738$  Å was selected using a Si(111) monochromator and focused on the sample using mirrors in the Kirkpatrick-Baez geometry. The diffraction patterns were recorded on a large area scanning MAR345 image plate and were analyzed using the FIT2D (Ref. 19) software package.

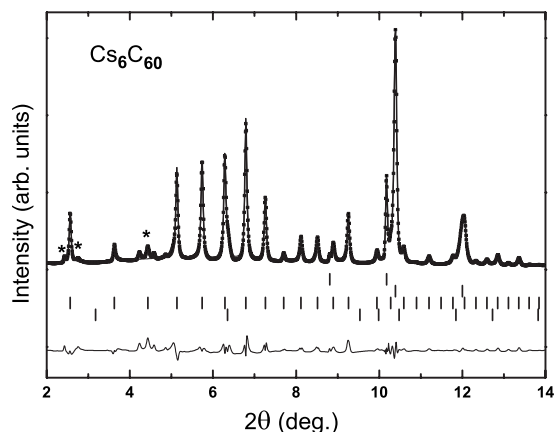


FIG. 1. Le Bail fit of the  $\text{Cs}_6\text{C}_{60}$  XRD pattern obtained in the high-pressure setup described in the text at room temperature and ambient pressure. The ticks correspond from top to bottom to MgO, CuBe alloy,  $\text{Cs}_6\text{C}_{60}$ , and graphite. The star labels point to peaks due to the B-epoxy gasket. The lower line corresponds to the residual pattern.

The sample to detector distance and the image plate tilt angles were precisely calibrated using a silicon standard located at the sample position.

XAS measurements were performed at the bending magnet BM29 beamline<sup>20</sup> in transmission geometry using a high-stability fixed-exit double-crystal Si(311) monochromator.

For pressure calibration, XRD patterns were collected by means of a MAR345 image plate detector mounted off axis with respect to the beam in analogy to the setup described in Ref. 21. The image plate position and the selected energy for XRD measurements have been chosen for each experimental run ( $\text{Cs}_6\text{C}_{60}$  and  $\text{Rb}_6\text{C}_{60}$ ) in order to optimize the detection of the most intense Debye-Scherrer rings of the pressure markers.

In both XRD and XAS experiments samples were inserted in CuBe alloy (2 wt % of Be) capsules, which were themselves embedded in a MgO cylinder and inserted in graphite (for  $\text{Cs}_6\text{C}_{60}$ ) or rhenium<sup>17</sup> (for  $\text{Rb}_6\text{C}_{60}$ ) resistive furnaces for the high-pressure-high-temperature measurements. The whole setup was prepared in an argon atmosphere glovebox in order to avoid sample deterioration. For each system the final sample environment was introduced in a 5 mm (external diameter) boron-epoxy gasket that was loaded between the anvils and precompressed in the glovebox before insertion in the Paris-Edinburgh cell. The diameter of the CuBe capsule containing the sample was equal to 1.5 mm (internal hole diameter of the gasket). Pressure calibration was done using the Vinet equations of state of NaCl and MgO.<sup>22,23</sup>

NaCl powder pellets were introduced on top and at the bottom of the CuBe capsule. In the particular case of XAS ambient temperature measurements on  $\text{Rb}_6\text{C}_{60}$  the experimental setup for the high-pressure cell was different. In this case we mixed small quantities of sample with the pressure marker (hBN) in the proportion  $\text{Rb}_6\text{C}_{60}:\text{BN}=1:13$  (in weight) and we inserted the mixture directly into the gasket without using the CuBe crucible. In this case only the hBN compound was used as pressure marker and the Birch-

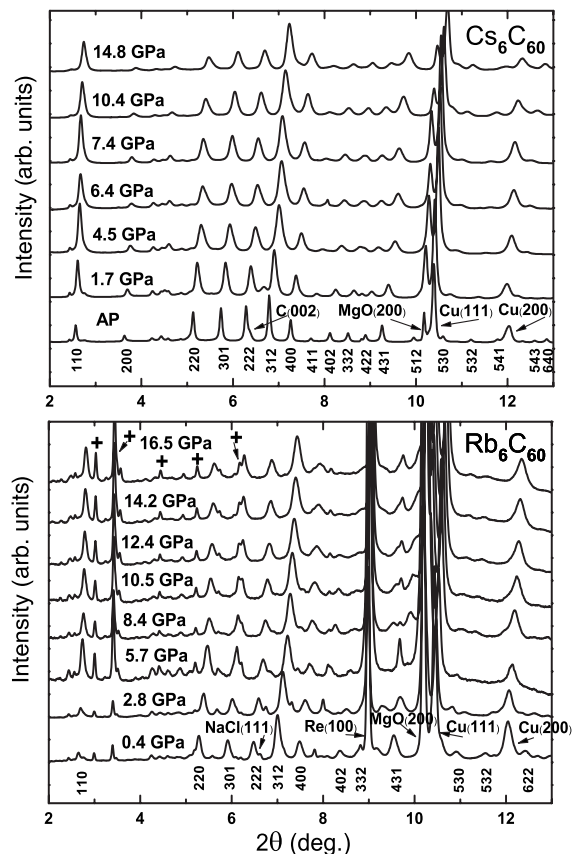


FIG. 2. Pressure evolution of the XRD pattern of  $\text{Cs}_6\text{C}_{60}$  (upper panel) and  $\text{Rb}_6\text{C}_{60}$  (lower panel) from ambient pressure (AP) up to 14.8 GPa and from 0.4 up to 16.5 GPa, respectively. Data have been normalized to the intensity of the (312) Bragg reflection. Labels denote the main Bragg peaks as well as reflections originating from the sample environment. “Cu” stands for the CuBe alloy capsule. In the lower panel some new Bragg reflections appearing at 5.7 GPa arise from the boron-epoxy gasket. They are indicated with the “+” symbol.

Murnaghan equation of state<sup>24</sup> was used to calibrate the pressure on the sample.

The high-temperature part of the experiments will be reported elsewhere. As  $\text{Cs}_6\text{C}_{60}$  and  $\text{Rb}_6\text{C}_{60}$  are extremely sensitive to oxygen and humidity, the pressure transmitting medium was previously oven dried and degassed in order to prevent contamination of the sample.

### III. EXPERIMENTAL RESULTS

#### A. X-ray diffraction

The data quality is illustrated by the Le Bail fitting of the  $\text{Cs}_6\text{C}_{60}$  sample at ambient pressure and room temperature inside the high-pressure environment cell presented in Fig. 1. The obtained fit allows us to guarantee the absence of sample contamination within our experimental protocol.

Both  $\text{Cs}_6\text{C}_{60}$  and  $\text{Rb}_6\text{C}_{60}$  systems present a body-centered cubic (bcc) structure ( $Im\bar{3}$  space group) at ambient conditions<sup>25</sup> where the fullerene molecules are centered on

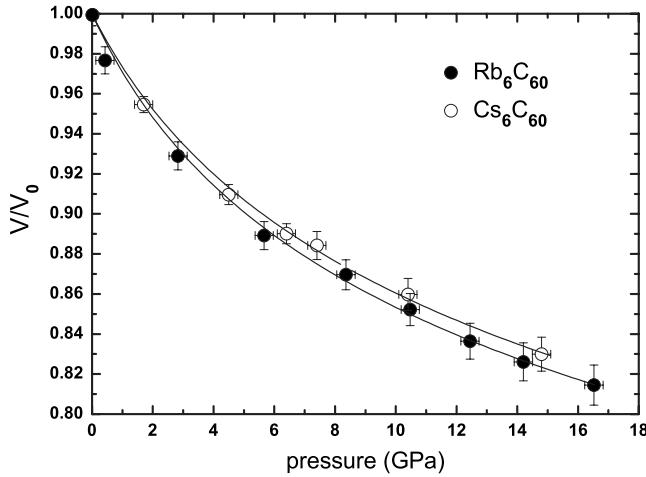


FIG. 3. Experimental pressure dependence of the volume of Cs<sub>6</sub>C<sub>60</sub> and Rb<sub>6</sub>C<sub>60</sub> relative to their ambient pressure values as obtained by XRD. We report the best fit curve of the Murnaghan equation of state function for the two systems.

the bcc Bravais lattice sites and the alkali metal atoms occupy all the 12 available tetrahedral sites of the host lattice. At room temperature and ambient pressure the values of lattice parameter of Cs<sub>6</sub>C<sub>60</sub> [ $a=11.790(1)$  Å] and Rb<sub>6</sub>C<sub>60</sub> [ $a=11.540(2)$  Å] obtained from our XRD analysis are in agreement with those reported in literature.<sup>15,25</sup>

The pressure evolution of the XRD patterns from ambient pressure up to 14.8 and 16.5 GPa, respectively, for Cs<sub>6</sub>C<sub>60</sub> and Rb<sub>6</sub>C<sub>60</sub> is shown in Fig. 2. No sign of phase transformation is observed up to the highest measured pressure.

Data were analyzed using the FULLPROF package<sup>26</sup> in the Le Bail configuration:<sup>27</sup> unit-cell parameters and profile shape parameters were fitted independently while the atomic coordinates have not been refined. Consequently, the XRD results obtained through the Le Bail refinement method can essentially determine the lattice parameter, the absence of detectable phase transition, and the sample purity.

Figure 3 shows the relative volume variation as a function of pressure obtained from the lattice parameters. The experimental value of the bulk modulus,  $B_0$ , and its pressure derivative,  $B'_0$ , were obtained by fitting the experimental volume vs pressure ( $V$  vs  $P$ ) points with the Murnaghan equation of state. The results are shown in Table I.

We obtain bulk modulus values of 30 and 33 GPa for Rb<sub>6</sub>C<sub>60</sub> and Cs<sub>6</sub>C<sub>60</sub>, respectively, and they coincide within the experimental error (Table I). This can be appreciated also in Fig. 3 where no straightforward conclusion about the relative compressibility of the two systems can be established due to experimental uncertainties.

Our obtained  $B_0$  value for Rb<sub>6</sub>C<sub>60</sub>, 30 GPa, is considerably smaller than the one experimentally found by Sabouri-Dodoran *et al.*<sup>15</sup> by studying the evolution of the lattice parameter on three Bragg reflections with no pressure transmitting medium. They obtained 55.4 and 54 GPa by using the Murnaghan and the Vinet equations of state, respectively. Due to the high correlation (0.98+) between  $B_0$  and its pressure derivative, it is important to consider that in our case  $B'_0$ , which is 8.5, is significantly higher than those obtained by Sabouri-Dodoran *et al.* (5.13 and 6.0 for the Murnaghan and Vinet, respectively). Nevertheless, the  $B_0$  value that we obtain is smaller compared to their values even if such correlation is taken into account.

In addition, we have also used the Vinet and the Birch-Murnaghan equations of state with results lying within our experimental uncertainty.

### B. Extended x-ray absorption fine structure

The XAS data were measured at the Cs  $K$ -edge (35.89 keV) and Rb  $K$ -edge (15.20 keV) for Cs<sub>6</sub>C<sub>60</sub> and Rb<sub>6</sub>C<sub>60</sub> from ambient pressure up to 15.7 and 8.2 GPa, respectively. The x-ray absorption near edge structure part of the spectra evolved smoothly in correspondence with the lack of phase transformation as confirmed by the XRD data. The extended x-ray absorption fine structure (EXAFS) data analysis of Cs<sub>6</sub>C<sub>60</sub> and Rb<sub>6</sub>C<sub>60</sub> was performed using the GNXAS package.<sup>28,29</sup> The extracted signals are shown in Fig. 4.

The evolution of the structural parameters of the first coordination shell as a function of pressure was obtained by fitting directly the absorption data without any noise filtering or preliminary background subtraction.

In the case of Rb<sub>6</sub>C<sub>60</sub>, the Rb  $K$ -edge double-electronic excitations<sup>30</sup> have been considered and kept fixed during the fitting procedure to the values obtained from the analysis of data at ambient pressure and room temperature where non-structural components are more clearly observable. In particular, the  $1s3d$  and  $1s3p$  double excitations corresponding

TABLE I. Bulk modulus  $B_0$  coefficients and its derivative  $B'_0$  of the two systems obtained from XRD data and *ab initio* calculations, of the C<sub>60</sub> molecule in the two different systems as obtained from *ab initio* calculations and of the interstitial volume ( $\langle M-C \rangle^3$ ) obtained from EXAFS data analysis. The errors of the quantities obtained from *ab initio* calculations correspond to the standard error of the best fit values while for the quantities obtained experimentally also the error propagation has been considered.

	Technique	Rb <sub>6</sub> C <sub>60</sub> $B_0$ (GPa)	Rb <sub>6</sub> C <sub>60</sub> $B'_0$	Cs <sub>6</sub> C <sub>60</sub> $B_0$ (GPa)	Cs <sub>6</sub> C <sub>60</sub> $B'_0$
Total volume	XRD	30 ( $\pm 3$ )	8.5 ( $\pm 0.5$ )	33 ( $\pm 3$ )	8.4 ( $\pm 0.5$ )
Total volume	Calculations	23 ( $\pm 1$ )	6.6 ( $\pm 0.2$ )	22 ( $\pm 3$ )	6.6 ( $\pm 0.2$ )
C <sub>60</sub> volume	Calculations	680 ( $\pm 20$ )	6.4	530 ( $\pm 18$ )	6.4
Interstitial volume	EXAFS	13 ( $\pm 3$ )	5	18 ( $\pm 3$ )	5

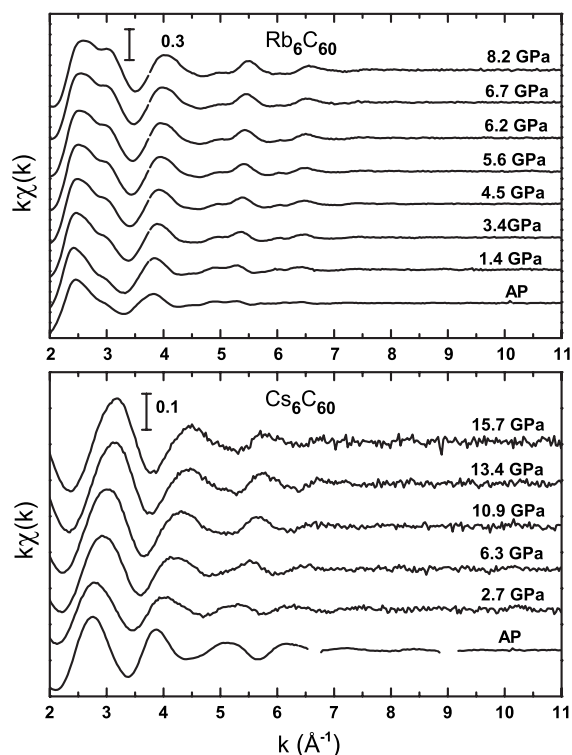


FIG. 4.  $k\chi(k)$  EXAFS signal as a function of pressure for  $\text{Rb}_6\text{C}_{60}$  at the Rb  $K$  edge (upper panel) and  $\text{Cs}_6\text{C}_{60}$  at the Cs  $K$  edge (lower panel).

to shake-off channels have been recognized in our data at  $\Delta E = E - E_0$  equal to 122.9 and 142 eV, respectively.

For both systems, the first coordination shell of each alkali atom consists of 22 C atoms, arranged in two hexagons and two pentagons facing the alkali metal and coming from four different molecules: two from the center and two from

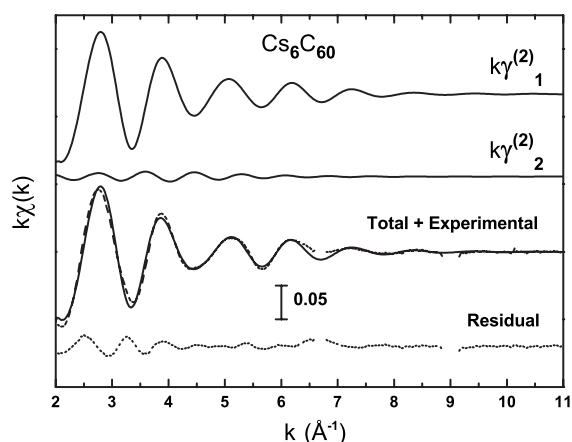


FIG. 5. EXAFS signal and fit of the Cs  $K$ -edge spectrum of  $\text{Cs}_6\text{C}_{60}$  at ambient conditions. The dashed line corresponds to the experimental signal with the continuous line overlapped corresponding to best fit.  $k\gamma_1^{(2)}$  and  $k\gamma_2^{(2)}$  are the contributions of the first 22 carbon neighbors and of the 4 first Cs neighbors, respectively. The missing experimental points around 6.7 and 9  $\text{\AA}^{-1}$  have been neglected because of the presence of glitches.

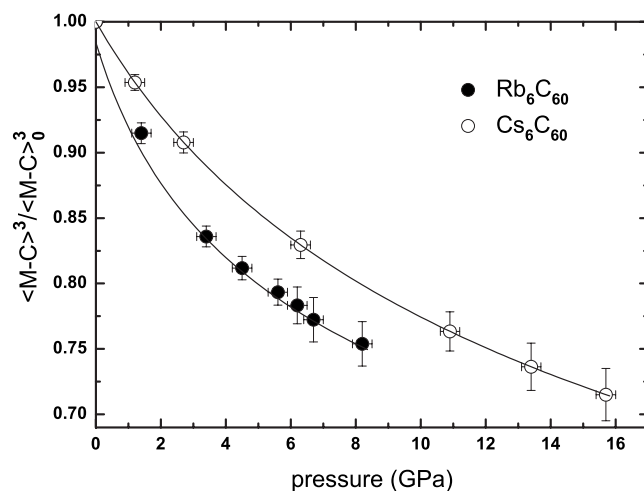


FIG. 6. Evolution of the interstitial volume of  $\text{Rb}_6\text{C}_{60}$  and  $\text{Cs}_6\text{C}_{60}$  relative to their ambient pressure values as obtained by the EXAFS analysis. We report the best fit curve of the Murnaghan equation of state function for the two systems.

the vertex sites in the bcc structure with respect to any tetrahedral site of alkali metal atom.

The second coordination shell consisting of four alkali metal atoms at distances of 4.114 and 4.194  $\text{\AA}$  (at ambient conditions) in  $\text{Rb}_6\text{C}_{60}$  and  $\text{Cs}_6\text{C}_{60}$ , respectively, was not considered in the fitting procedure for data under pressure because the data quality is not sufficient to include such contribution.

The EXAFS signal of  $\text{Cs}_6\text{C}_{60}$  at ambient pressure and room temperature and the best fit are reported in Fig. 5. The missing experimental points around 6.7 and 9  $\text{\AA}^{-1}$  have been neglected because of the presence of monochromator-induced glitches. The calculated total signal takes into account the first 22 carbon neighbor and first 4 Cs neighbor contributions, labeled  $k\gamma_1^{(2)}$  and  $k\gamma_2^{(2)}$ , respectively.

For both systems,  $\text{Rb}_6\text{C}_{60}$  and  $\text{Cs}_6\text{C}_{60}$ , the pressure evolution of the first coordination shell has been studied considering an asymmetric distribution of these C atoms around each alkali metal photoabsorber Rb and Cs atom.

Phases and amplitudes of the EXAFS signals were generated by considering a cluster of 22 carbon atoms and 4 alkali metal atoms around the photoabsorber. Different clusters derived from the compressed structure obtained by our *ab initio* calculations were used as initial inputs for the analysis of the spectra at different pressures.

In Fig. 6 we report the relative evolution of the “interstitial” volume (between the fullerenes) in the bcc structures of  $\text{Rb}_6\text{C}_{60}$  and  $\text{Cs}_6\text{C}_{60}$ . Such volume is obtained by considering a sphere having a radius equal to the EXAFS average distance between the alkali metal and its first neighbor shell of 22 carbon atoms.

We calculated the bulk modulus coefficients of such interstitial volume for the two compounds by fitting the experimental values  $V$  vs  $P$  obtained by the EXAFS analysis with the Murnaghan equation of state (Table I).

We can observe that the interstitial volume in the  $\text{Rb}_6\text{C}_{60}$  system is more compressible than in  $\text{Cs}_6\text{C}_{60}$ . They have  $B_0$



values of 13 and 18 GPa, respectively. The  $B'_0$  coefficient has been fixed to 5, which is the average value between those obtained for the two systems which were 4 and 6 for Rb<sub>6</sub>C<sub>60</sub> and Cs<sub>6</sub>C<sub>60</sub>, respectively. The choice of a common value of  $B'_0$  for both systems allows for a congruent comparison of the compressibility values due to the high correlation between  $B_0$  and its pressure derivative as discussed in Sec. III A.

#### IV. AB INITIO CALCULATIONS

We have performed density functional *ab initio* simulations of the two systems under high pressure.

In particular, we have used the SIESTA (Ref. 31) method, where the eigenstates of the Kohn-Sham Hamiltonian are expressed as linear combinations of numerical atomic orbitals. We have used variationally optimized<sup>32,33</sup> double- $\zeta$  polarized basis sets. Real space integrals were performed on a mesh with a 310 Ry cutoff.

We worked within the local density approximation to the exchange and correlation potential.<sup>34</sup>

Core electrons are replaced by nonlocal, norm-conserving fully separable Troullier-Martins pseudopotentials. In the calculations 2s and 2p orbitals of C atoms were explicitly included in the valence. For the Rb and Cs atoms, we included both semicore and valence orbitals, the 5s and 4p and the 6s and 5p, respectively. For Cs atoms, in particular, the inclusion of both semicore and valence orbitals was found to be critical in order to correctly predict the structural properties of this compound.

The bcc unit cell contains a total of 66 atoms and sampling of the reciprocal space was performed using a  $2 \times 2 \times 2$  Monkhorst-Pack mesh.

We studied the structural and electronic evolutions of Rb<sub>6</sub>C<sub>60</sub> and Cs<sub>6</sub>C<sub>60</sub> as a function of pressure by decreasing the lattice parameter from the experimental value found at ambient pressure and room temperature ( $a=11.54$  Å and  $a=11.79$  Å)<sup>15</sup> down to 10.70 and 11.00 Å, respectively. This corresponds to the following pressure range:  $[-1.8; 15.7]$  GPa for Rb<sub>6</sub>C<sub>60</sub> and  $[-1.2; 14.3]$  GPa for Cs<sub>6</sub>C<sub>60</sub>. The negative values of pressure corresponding to the experimental lattice parameters found at ambient conditions are a result of the well known DFT-LDA underestimation of the experimental lattice constant.

For the different values of the volume we have minimized the total energy until the forces on atoms were smaller than 0.04 eV/Å.

Both the structural and electronic evolutions of the two systems confirm the phase stability observed experimentally up to 8.2 and 15.7 GPa for the Rb<sub>6</sub>C<sub>60</sub> and Cs<sub>6</sub>C<sub>60</sub> compounds, respectively.

Both systems are insulators at low pressure with the  $t_{1u}$  three-fold degenerate state completely occupied and a gap between the highest occupied and the lowest unoccupied bands of 0.66 and 0.63 eV for Cs<sub>6</sub>C<sub>60</sub> and Rb<sub>6</sub>C<sub>60</sub>, respectively. The electronic structure shows a progressive closure of this gap as a function of pressure resulting from the bandwidth broadening consistent with the increase in density. In Fig. 7 we report the evolution of the gap and the evolution of the bandwidth of the  $t_{1u}$  (highest occupied) band and  $t_{1g}$  (lowest occupied) band for both systems as a function of

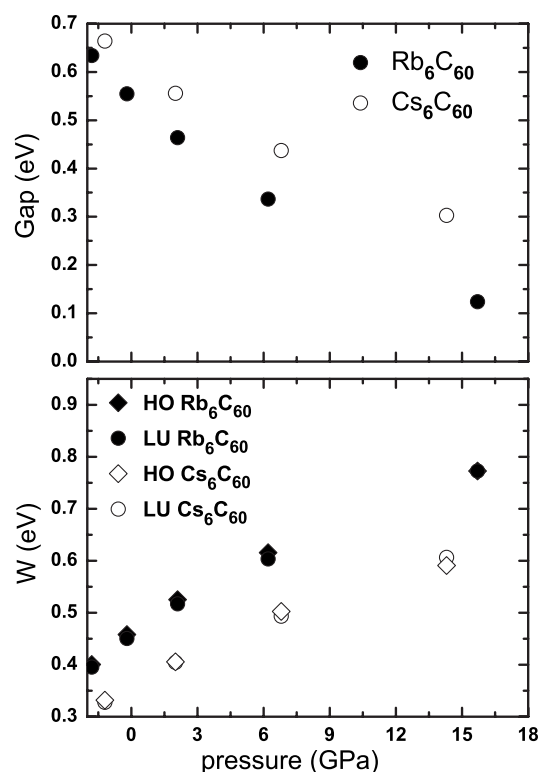


FIG. 7. Electronic structure evolution of the two systems as a function of pressure. The evolution of the calculated gap (upper panel) between the highest occupied (HO) and the lowest unoccupied (LU) bands and the bandwidth  $W$  (lower panel) as a function of pressure is shown in the picture for both systems. The rhombus symbol in the lower panel corresponds to the HO band values.

pressure. These data show the evidence of a pressure-induced metallization which should apply in the absence of structural phase transformations.

In Fig. 8 we show the two  $E(V)$  calculated curves. They have been fitted by using the Murnaghan equation of state. The obtained coefficients are reported in Table I. We observe that even if the compressibility values of Rb<sub>6</sub>C<sub>60</sub> (23 GPa) and Cs<sub>6</sub>C<sub>60</sub> (22 GPa) are different from those obtained experimentally, they coincide for the two systems within the error and such result is in close agreement with our experimental observations. However, this is in contradiction with the theoretical work of Ranjan *et al.*<sup>35</sup> where they found bulk moduli of 52.5 and 38.2 GPa for Rb<sub>6</sub>C<sub>60</sub> and Cs<sub>6</sub>C<sub>60</sub>, respectively.

The C<sub>60</sub> molecule compressibility has been studied in the two different systems. While we cannot partition the total energy of the system into two separated C<sub>60</sub> and alkaline contributions, we can estimate the C<sub>60</sub> compressibility by considering the variations of the total energy of the Rb<sub>6</sub>C<sub>60</sub> and Cs<sub>6</sub>C<sub>60</sub> structures as a function of the molecule volume. The volume of the C<sub>60</sub> molecule is calculated numerically as a discrete integral of the space enclosed by the 60 C atoms. This is computed in the real grid built in the SIESTA calculation. The  $E(V)$  curves are shown in Fig. 8. The compressibility coefficients have been obtained by fitting the  $E$  vs  $V$  points with the Murnaghan equation of state and the result is

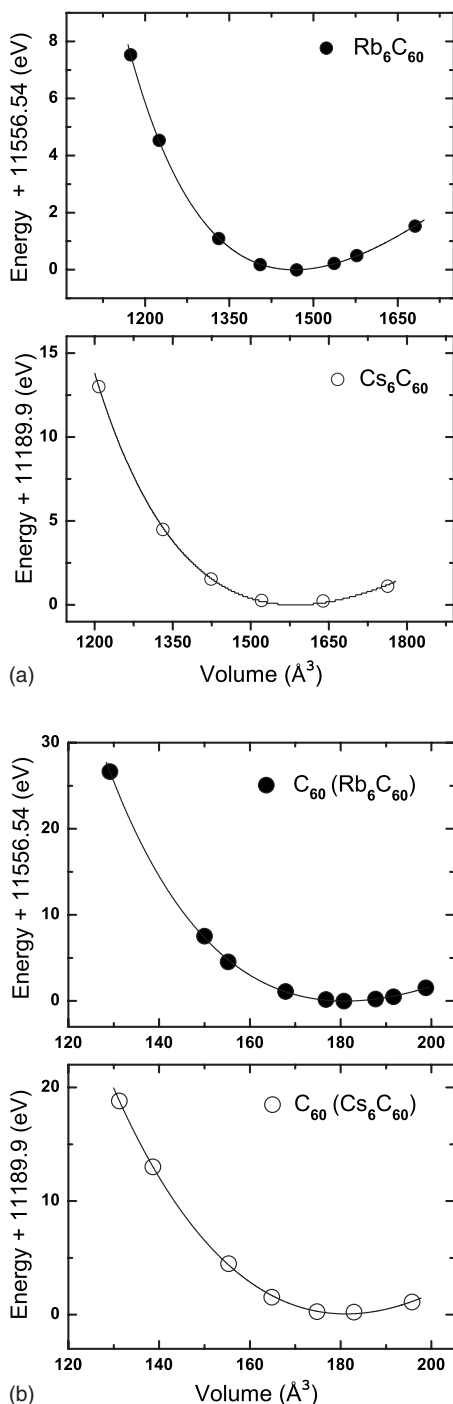


FIG. 8. Calculated total energy versus volume for  $\text{Rb}_6\text{C}_{60}$  (upper left panel),  $\text{Cs}_6\text{C}_{60}$  (lower left panel),  $\text{C}_{60}$  molecule in the  $\text{Rb}_6\text{C}_{60}$  (upper right panel), and  $\text{Cs}_6\text{C}_{60}$  (lower right panel) structure. The continuous line is a fit of the calculated  $E(V)$  points by the Murnaghan equation of state.

reported in Table I. The  $\text{C}_{60}$  molecule belonging to  $\text{Rb}_6\text{C}_{60}$  shows a bulk modulus (680 GPa) coefficient higher than for  $\text{Cs}_6\text{C}_{60}$  (530 GPa). Even though these values are smaller than those previously reported for the isolated molecule,<sup>1,2</sup> a meaningful comparison cannot be carried out due to our method used for the estimation of the bulk modulus. Nevertheless, the comparison of the compressibility between the

two systems, calculated within the same approximation, can be, in principle, fairly made.

## V. RESULTS AND DISCUSSION

Important considerations arise by considering the different experimental and theoretical bulk moduli given in Table I. We should be aware that some of the compressibilities here defined do not correspond to the thermodynamic ones, as they have a local character. Nevertheless, their use has already been found to be extremely useful in the study of isotropic<sup>36</sup> as well as in anisotropic systems.<sup>37</sup>

By considering the geometric volume of the fullerene,  $V_F$ , the total volume of the bcc fulleride cell,  $V_T$ , of the two  $\text{M}_6\text{C}_{60}$  systems can be decomposed as

$$V_T = 2V_F + nV_i, \quad (1)$$

where  $nV_i$  represents the total interstitial volume in the bcc unit cell.

We have defined then a volume corresponding to the average distance between the alkali metal atom and the first 22 carbon atom neighbors as we did in EXAFS, which corresponds to  $nV_i$ . The evaluation from *ab initio* calculations of all the variables in Eq. (1), i.e.,  $V_T$ ,  $V_F$ , and  $V_i$ , leads to a value of  $n$  equal to 22. By deriving and opportunely reorganizing Eq. (1) we can then conclude that with a 1% uncertainty, coming from the fact that we neglect the term associated with the fullerene molecule due to its low compressibility,

$$\frac{B_{0T}}{B_{0i}} = \frac{V_{0T}}{V_{0T} - 2V_{0F}}, \quad (2)$$

where the  $T$  and  $F$  labels apply again to total and fullerene, respectively.

By using the right side term of Eq. (2), we obtain a value of approximately 1.3 for both systems. This value differs from the ones that can be obtained by evaluation of the left side of Eq. (2) using the experimental data in (Table I) which give 2.3 for  $\text{Rb}_6\text{C}_{60}$  and 1.8 for  $\text{Cs}_6\text{C}_{60}$ . This represents a difference of 78% and 41%, respectively, with respect to the result from the other part of the equation. Consequently we need to conclude that the interstitial volume given by EXAFS decreases too rapidly to be considered as representing the real interstitial volume. In addition, such volume reduction appears to be more important in the Rb than in the Cs intercalation case.

In order to explain such disagreement, we consider the evolution of the geometry of the molecule with pressure as given by our *ab initio* calculations. In Fig. 9 we show the histogram plot of the evolution with pressure of the distance of the carbon atoms from the geometric center of the molecule in  $\text{Rb}_6\text{C}_{60}$  and  $\text{Cs}_6\text{C}_{60}$ .

While in the isolated  $\text{C}_{60}$  molecule with  $I_h$  symmetry all C atoms are equidistant from the center, in the studied fullerides the fullerene molecule exhibits a bimodal distribution of distances. This dispersion encountered in the case of the alkali intercalated fullerenes, which characterizes a deformation with respect to the icosahedral symmetry, is further en-

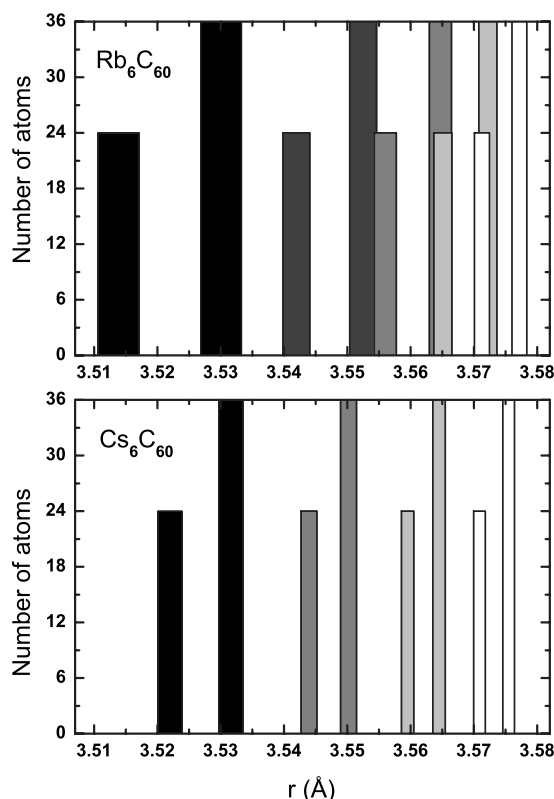


FIG. 9. Histograms of the  $\rho$  distribution for the molecule in the  $Rb_6C_{60}$  (upper panel) and  $Cs_6C_{60}$  systems (lower panel), for the different pressure values, respectively. We report histograms for  $-1.8, -0.2, 2, 6.2,$  and  $15.7$  GPa and  $-1.2, 2, 6.8,$  and  $14.3$  GPa, for  $Rb_6C_{60}$  and  $Cs_6C_{60}$ , respectively, starting from the right side of the graphs. The histograms are reported within a spacing between bars equal to 60% meaning that more dispersed distributions are represented with wider columns.

hanced under pressure. It corresponds to an elongation of the  $C_{60}$  cage along the three Cartesian axes and confirms previous studies carried out on  $Rb_6C_{60}$  and  $K_6C_{60}$ .<sup>11</sup> The origin of the important distortion of the  $C_{60}$  molecule in these alkali intercalated compounds can probably be found on the ionic interaction between the fullerene and the intercalated ions.

Let us call  $\rho$  the distance of the C atoms from the center of the molecule. We consider then the difference between  $\rho$  of each atom and the  $\rho_{av}$  quantity obtained as the average between the 60  $\rho$  values. With pressure, the distance of the 60 C atoms from the center decreases and the  $C_{60}$  molecule preserves the same distribution of  $\rho$ , namely, 36 atoms at  $\rho_p > \rho_{av}$  and 24 with  $\rho_n < \rho_{av}$ . Nevertheless, the shape of such distribution evolves differently for  $Rb_6C_{60}$  and for  $Cs_6C_{60}$ , as shown in Fig. 9.

We can then define a distortion parameter  $d$  as follows:

$$d = \frac{1}{36} \sum_{i=1}^{36} \rho_p(i) - \frac{1}{24} \sum_{i=1}^{24} \rho_n(i). \quad (3)$$

In Fig. 10 we plotted the fullerene distortion parameter  $d$  as a function of pressure for both  $Rb_6C_{60}$  and  $Cs_6C_{60}$ . It increases with pressure in both cases and for all pressures the

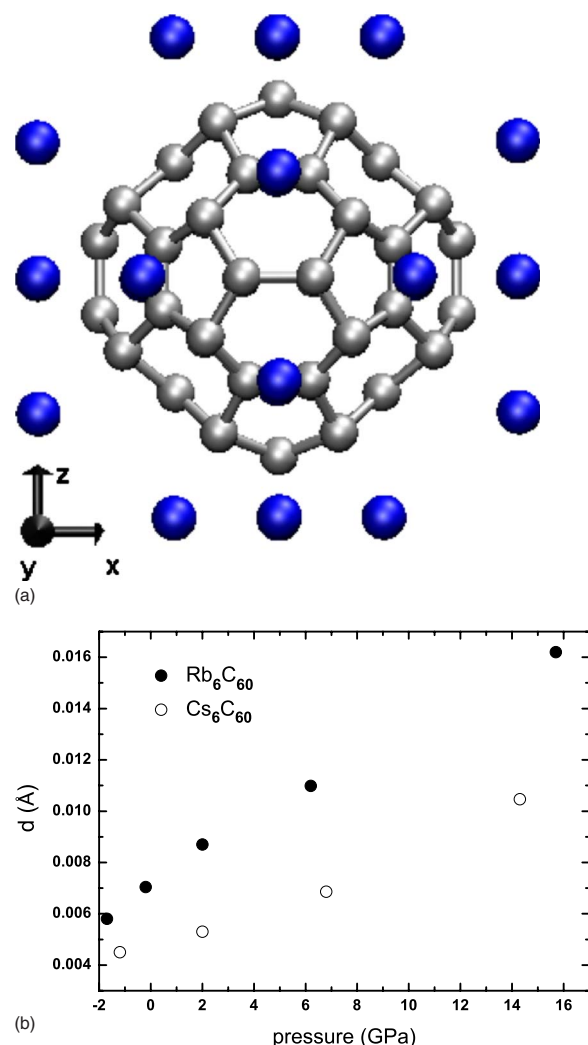


FIG. 10. (Color online) Pressure-induced distortion of  $C_{60}$ . The distorted  $C_{60}$  molecule is represented with the 24 Rb atoms at the tetrahedral sites (upper panel). We report the molecule at 15.7 GPa with an enhanced distortion such that  $d$  has been increased of a factor 32. The evolution of the difference between the average value of  $\rho_p$  and the average value of  $\rho_n$  for the different pressure conditions of the relative system is reported in the lower panel.

distortion induced by Rb intercalation is higher than for the Cs case.

At the highest pressure studied, i.e., around 15 GPa,  $d$  becomes 2.8 and 2.3 times higher (for  $Rb_6C_{60}$  and  $Cs_6C_{60}$ , respectively) compared to the low pressure case corresponding to the experimental value of the lattice parameter found at ambient pressure. This corresponds to a 54% higher distortion of the molecule in  $Rb_6C_{60}$  compared to  $Cs_6C_{60}$ .

The nature of the pressure-induced distortion can be understood by looking at the upper panel of Fig. 10 where we represent the  $C_{60}$  molecule in the bcc  $Rb_6C_{60}$  structure surrounded by 24 Rb atoms placed at the tetrahedral sites at the 6 faces. In this picture, the  $d$  parameter has been amplified by a factor of 32 in order to better appreciate the pressure-induced deformation. The pressure-induced distortion constitutes basically an amplification of the one already observed at ambient conditions. In conclusion, the shape modification

of the  $C_{60}$  fullerene can be better interpreted as an elongation of the molecule due to a traction force, in which the molecule is pulled in the three Cartesian axes probably due to the Coulombic interaction between the negatively charged fullerene and the alkali cations. The observed distortion is considerably smaller than that observed for the buckminsterfullerene in single crystal of 3D polymers of undoped  $C_{60}$  by Yamanaka *et al.*<sup>8</sup> They observed a cuboidal molecule at ambient pressure with the distortion parameter, according to Eq. (3), equal to 0.6, i.e., 37 and 57 times higher than the distortion of the fullerene in  $Rb_6C_{60}$  and  $Cs_6C_{60}$ , respectively, calculated by us at around 15 GPa. This is essentially due to the formation of strong covalent bondings between the molecules in the 3D polymerized structure.

We can now understand the apparent inconsistency that we found when comparing the two terms of Eq. (2). The pressure-induced deformation of the  $C_{60}$  molecule leads to an additional reduction of the alkali-carbon distances that needs to be added to simple homogenous compressive effects.

In addition, our calculations show that the deformation of the fullerene in the case of Rb intercalation is stronger than for Cs, consistently with local compressibilities obtained by EXAFS, where higher interstitial volume compressibility is obtained for  $Rb_6C_{60}$  ( $B_0=13$  GPa) with respect to  $Cs_6C_{60}$  ( $B_0=18$  GPa). Moreover, although the molecule in  $Rb_6C_{60}$  appears to suffer a stronger deformation than in  $Cs_6C_{60}$ , its stiffness ( $B_0=680$  GPa) is interestingly higher than in the case of Cs intercalation ( $B_0=530$  GPa) as obtained by *ab initio* calculations.

## VI. CONCLUSIONS

We have reported a detailed study of the  $Rb_6C_{60}$  and  $Cs_6C_{60}$  systems under pressure. In particular, we coupled the complementary information obtained by XRD and EXAFS with the result obtained by *ab initio* calculations in order to understand the mechanisms taking place during the compression of such systems.

We have calculated and measured the compressibility of both systems and compared this to that obtained by EXAFS for the interstitial volumes between molecules. Both for  $Rb_6C_{60}$  and  $Cs_6C_{60}$  the EXAFS compressibilities appear to be too small to correspond to an isotropic compression of the system. The analysis of the pressure-induced deformation of the  $C_{60}$  molecule via *ab initio* calculations allows us to understand such differences.

We infer that compression of the  $C_{60}$  molecule is accompanied by a shape-changing deformation under pressure. This is probably due to an enhancement of the Coulombic interaction with the surrounding ions, effectively increasing the difference between the distances from each molecule's center to those 36 carbons closest to the alkali metals, on one hand, and to those 24 carbon atoms located closest to other  $C_{60}$  molecules, on the other. This deformation is analogous to pulling the molecule through the three orthogonal axes pointing toward the bcc faces containing the alkali metals.

Both experiments and calculations agree with a deformation of the fullerene molecule which is more important for Rb than for Cs intercalation. The defined distortion parameter of the fullerene,  $d$ , obtained by analyzing the evolution of both structures under pressure, is 54% higher in  $Rb_6C_{60}$  than in  $Cs_6C_{60}$  at around 15 GPa. This fact cannot be simply associated with steric effects because of the higher stiffness of the molecule, obtained by our calculation, in the Rb than in the Cs intercalated system.

## ACKNOWLEDGMENTS

Part of this work was supported by the French Ministère Délégué à la Recherche et aux Nouvelles Technologies and the CNRS through grants "ACI-2003 No. NR0122" and "ACI-2003 No. JC2077." The authors thank H. Feret and S. Pasternak for their assistance and technical support. M.V.F.-S. acknowledges funding from the Marie Curie EXT project MEXT-CT-2005-023311. Beamtime allocated to proposal HS3025 at ID27, ESRF.

- <sup>1</sup>S. J. Woo, S. H. Lee, E. Kim, K. H. Lee, Y. H. Lee, S. Y. Hwang, and I. C. Jeon, *Phys. Lett. A* **162**, 501 (1992).
- <sup>2</sup>R. S. Ruoff, *Nature (London)* **350**, 663 (1991).
- <sup>3</sup>M. Núñez-Regueiro, L. Marques, J.-L. Hodeau, O. Bèthoux, and M. Perroux, *Phys. Rev. Lett.* **74**, 278 (1995).
- <sup>4</sup>L. Marques, M. Mezouar, J.-L. Hodeau, M. Núñez-Regueiro, N. R. Serebryanaya, V. A. Ivdenko, V. D. Blank, and G. A. Dubitsky, *Science* **283**, 1720 (1999).
- <sup>5</sup>B. Sundqvist, *Adv. Phys.* **48**, 1 (1999).
- <sup>6</sup>R. Moret, *Acta Crystallogr., Sect. A: Found. Crystallogr.* **61**, 62 (2005).
- <sup>7</sup>A. San Miguel, *Chem. Soc. Rev.* **35**, 876 (2006).
- <sup>8</sup>S. Yamanaka, A. Kubo, K. Inumaru, K. Komaguchi, N. S. Kini, T. Inoue, and T. Irifune, *Phys. Rev. Lett.* **96**, 076602 (2006).
- <sup>9</sup>A. M. Rao, P. C. Eklund, J.-L. Hodeau, L. Marques, and M. Núñez-Regueiro, *Phys. Rev. B* **55**, 4766 (1997).
- <sup>10</sup>M. Mezouar, L. Marques, J.-L. Hodeau, V. Pischedda, and M.

- Núñez-Regueiro, *Phys. Rev. B* **68**, 193414 (2003).
- <sup>11</sup>W. Andreoni, F. Gygi, and M. Parrinello, *Phys. Rev. Lett.* **68**, 823 (1992).
- <sup>12</sup>M. S. Dresselhaus, G. Dresselhaus, and P. C. Eklund, *Science of Fullerenes and Carbon Nanotubes* (Academic, New York, 1996).
- <sup>13</sup>B. Verbeck, H. Michel, and A. V. Nikolaev, *J. Chem. Phys.* **23**, 10462 (2002).
- <sup>14</sup>R. Röding, T. Wågberg, and B. Sundqvist, *Chem. Phys. Lett.* **413**, 157 (2005).
- <sup>15</sup>A. A. Sabouri-Dodaran, M. Marangolo, C. Bellin, F. Mauri, G. Figuet, G. Loupiau, M. Mezouar, W. Crichton, C. Hérold, F. Rachdi, and S. Rabii, *Phys. Rev. B* **70**, 174114 (2004).
- <sup>16</sup>J. M. Besson, R. J. Nemes, G. Hamel, J. S. Loveday, G. Weill, and S. Hull, *Physica B* **180&181**, 907 (1992).
- <sup>17</sup>G. Morard, M. Mezouar, N. Rey, R. Poloni, A. Merlen, S. Le Floch, P. Toulemonde, S. Pascarelli, A. San Miguel, C. Sanloup



- and G. Fiquet, *High Press. Res.* **27**, 223 (2007).
- <sup>18</sup>M. Mezouar, W. A. Crichton, S. Bauchan, F. Thurel, H. Witsch, F. Torrecillas, G. Blattmann, P. Marion, Y. Dabin, J. Chavanne, O. Hignette, C. Morawe, and C. Borel, *J. Synchrotron Radiat.* **12**, 659 (2005).
- <sup>19</sup>D. P. Hammersley, S. O. Svensson, M. Hanfland, A. N. Fitch, and D. Hausermann, *High Press. Res.* **14**, 235 (1996).
- <sup>20</sup>A. Filipponi, M. Borowski, D. T. Bowron, S. Ansell, A. Di Cicco, S. De Panfilis, and J.-P. Itié, *Rev. Sci. Instrum.* **71**, 2422 (2000).
- <sup>21</sup>G. Aquilanti, W. Crichton, and S. Pascarelli, *High Press. Res.* **23**, 301 (2003).
- <sup>22</sup>P. Vinet, J. R. Smith, J. Ferrante, and J. H. Rose, *Phys. Rev. B* **35**, 1945 (1987).
- <sup>23</sup>Y. Le Godec, D. Martinez-Garcia, M. Mezouar, G. Syfosse, J.-P. Itié, and J.-M. Besson, *High Press. Res.* **18**, 339 (2000).
- <sup>24</sup>Y. Le Godec, D. Martinez-Garcia, M. Mezouar, G. Syfosse, J.-P. Itié, and J.-M. Besson, *Proceeding of AIRAPT-17*, edited by M. H. Manghnani, W. J. Nellis, and M. F. Nicol (Eds.), Universities Press, Hyderabad, p. 925, (2000).
- <sup>25</sup>O. Zhou and D. E. Cox, *J. Phys. Chem. Solids* **53**, 1373 (1992).
- <sup>26</sup>J. Rodriguez-Carvajal, *Physica B* **192**, 55 (1993).
- <sup>27</sup>A. Le Bail, H. Duroy, and J. L. Fourquet, *Mater. Res. Bull.* **23**, 447 (1988).
- <sup>28</sup>A. Filipponi, A. Di Cicco, and C. R. Natoli, *Phys. Rev. B* **52**, 15122 (1995).
- <sup>29</sup>A. Filipponi and A. Di Cicco, *Phys. Rev. B* **52**, 15135 (1995).
- <sup>30</sup>A. Kodre, I. Arčon, J. P. Gomilsek, R. Prešeren, and R. Frahm, *J. Phys. B* **35**, 3497 (2002).
- <sup>31</sup>J. M. Soler, E. Artacho, J. D. Gale, A. García, J. Junquera, P. Ordejón, and D. S. Sanchez-Portal, *J. Phys.: Condens. Matter* **14**, 2745 (2002).
- <sup>32</sup>J. Junquera, O. Paz, D. Sánchez-Portal, and E. Artacho, *Phys. Rev. B* **64**, 235111 (2001).
- <sup>33</sup>E. Anglada, J. M. Soler, J. Junquera, and E. Artacho, *Phys. Rev. B* **66**, 205101 (2002).
- <sup>34</sup>J. P. Perdew and A. Zunger, *Phys. Rev. B* **23**, 5048 (1981).
- <sup>35</sup>K. Ranjan, K. Dharamvir, and V. K. Jindal, *Indian J. Pure Appl. Phys.* **43**, 654 (2005).
- <sup>36</sup>A. San-Miguel, A. Polian, M. Gauthier, and J. P. Itié, *Phys. Rev. B* **48**, 8683 (1993).
- <sup>37</sup>J. Pellicer-Porres, A. Segura, V. Muñoz, and A. San Miguel, *Phys. Rev. B* **60**, 3757 (1999).